*This is a preprint of an article published in Molecular Plant. The final authenticated version is available online at: https://doi.org/10.1016/j.molp.2022.08.008*

# The regeneration factors ERF114 and ERF115 regulate auxin mediated lateral root development in response to mechanical cues

Balkan Canher[1,2], Fien Lanssens[1,2], Ai Zhang[3], Anchal Bisht[1,2], Shamik Mazumdar[3], Jefri Heyman[1,2], Sebastian Wolf[4], Charles W. Melnyk[3] and Lieven De Veylder[1,2,*]

[1]Department of Plant Biotechnology and Bioinformatics, Ghent University, Ghent, B-9052, Belgium. [2]VIB Center for Plant Systems Biology, Ghent, B-9052, Belgium.

[3]Department of Plant Biology, Linnean Center for Plant Biology, Swedish University of Agricultural Sciences, Almas allé 5, 756 51, Uppsala, Sweden.

[4]Department of Plant Biochemistry, Center for Plant Molecular Biology (ZMBP), University of Tübingen, 72076 Tübingen, Germany

* Corresponding author: De Veylder, Lieven

**Email:** lieven.deveylder@psb.vib-ugent.be

**ORCID IDs:**

0000-0001-5118-4178 (B.C.); 0000-0002-1698-1355 (F.L.); 0000-0002-8308-9973 (A.Z.); 0000-0003-4290-6647 (A.B.); 0000-0002-7319-1069 (S.M.); 0000-0003-3266-4189 (J.H.); 0000-0003-0832-6315 (S.W.); 0000-0003-3251-800X (C.W.M.); 0000-0000-0003-1150-4426 (L.D.V.)

**One-Sentence Summary:**

Mechanical Cues Drive *ERF114/ERF115* expression during lateral root development as well as regeneration.

**Corresponding author:**

Lieven De Veylder

VIB Center for Plant Systems Biology

Ghent University, Department of Plant Biotechnology and Bioinformatics

Technologiepark 71

B-9052 Gent (Belgium)

Tel.: +32 9 3313961; Fax: +32 9 3313809; E-mail: lieven.deveylder@psb.vib-ugent.be

**ABSTRACT**

Plants show an unparalleled regenerative capacity, allowing them to survive severe stress conditions, such as injury, herbivory attack and harsh weather conditions. This potential not only replenishes tissues and restores damaged organs, but can also give rise to whole plant bodies. Despite the intertwined nature of development and regeneration, upstream cues and signaling mechanisms that commonly activate organogenesis are largely unknown. Here, we demonstrate that next to being activators of regeneration*, ETHYLENE RESPONSE FACTOR 114* (*ERF114*) and *ERF115* govern developmental growth in the absence of wounding or injury. Increased *ERF114* and *ERF115* activity enhances auxin sensitivity, which is correlated with enhanced xylem maturation and lateral root formation, whereas their knockout results in a decrease in lateral roots. Moreover, we provide evidence that mechanical cues contribute to *ERF114* and *ERF115* expression in correlation with BZR1-mediated brassinosteroid signaling under both regenerative and developmental conditions. Antagonistically, cell wall integrity surveillance via mechanosensory FERONIA signaling suppresses their expression under both conditions. Our data suggest a molecular framework in which cell wall signals and mechanical strains regulate organ development and regenerative responses via ERF114 and ERF115 mediated auxin signaling.

## INTRODUCTION

While inherited genetic and molecular information in plants and animals orchestrate the unfolding of developmental processes with high precision, strategies to cope with unexpected loss of cells or organs through wounding are essential for survival and continuity of any species. Due to their immobile nature, plants have developed mechanisms that allow the organism to instantly detect the nature and extent of injury and activate the precise regenerative mechanisms needed for each of the numerous scenarios of injury. Stem cell death, meristem incision or targeted wounding such as loss of a few cells upon laser ablation, locally reactivate the developmental signaling pathways that allow replacement of the lost cells in a precise and functional manner (Birnbaum and Sanchez Alvarado, 2008; Canher et al., 2020; Melnyk et al., 2015; Savatin et al., 2014). Interestingly, regenerative signaling networks governing callus formation are activated during lateral root formation, leading to regeneration and development being described as two sides of the same coin (Perianez-Rodriguez et al., 2014).

The ERF subfamily X transcription factors (ERF108-115) has been suggested to play an emerging role in diverse regenerative processes (Heyman et al., 2018). ERF115 was initially identified as a driver of quiescent center stem cell divisions during development (Heyman et al., 2013). Since the discovery that death of a single cell triggers *ERF115* expression in neighboring cells and subsequently pushes them to initiate a cell division program, it has been studied extensively within the context of wounding and regeneration (Heyman et al., 2016; Hoermayer et al., 2020; Marhava et al., 2019; Zhou et al., 2019). Expression of *ERF115* after DNA damage-induced stem cell death was found to act synergistically with a wound-induced accumulation of auxin, which in turn allows the

damaged cells to be replaced by new cells (Canher *et al.*, 2020). The synergistic effect of ERF115 on auxin signaling was reported to be due to activation of *MONOPTEROS* (*MP*), a member of the *AUXIN RESPONSE FACTOR* (*ARF)* family. *MP* has been shown to be essential for many developmental and regenerative processes including maintenance and formation of meristems, vascular development, leaf blade formation as well as shoot and root regeneration (Bhatia et al., 2016; Ckurshumova et al., 2014; Efroni et al., 2016; Jürgens, 1993; Krogan et al., 2016; Luo et al., 2018; Przemeck et al., 1996; Schuetz et al., 2008). On top of that and similar to its role in primary meristems, MP-mediated auxin signaling and transport tightly controls virtually every stage of LR development (De Smet et al., 2010).

ERF114, the closest homolog of ERF115, is also known as ERF BUD ENHANCER (EBE) because of the observed increased axillary bud outgrowth upon its overexpression (Mehrnia et al., 2013). Its expression is strongly induced following wounding and coincides with callus formation at the cut sites. A prominent feature observed upon *ERF114* overexpression is neoplasia in the form of tissue that is similar to green callus, which is often produced at wound sites. Moreover, it has been observed that tissue explants derived from *ERF114* overexpressing plants display increased rates of callus production when cultured on callus-inducing medium (Mehrnia *et al.*, 2013).

Even though the involvement of ERF subfamily X transcription factors in wounding and regeneration is well established, the mechanism leading to their activation upon wounding has not been agreed upon. Activation of a jasmonate acid (JA) signaling network acting in synergy with auxin was reported to cause *ERF115* induction upon wounding or nematode infection (Zhou *et al.*, 2019). Similarly, *ERF109* was shown to be activated by

JA and promote lateral root formation by activating auxin biosynthesis (Cai et al., 2014). Furthermore, reactive oxygen species were shown to control the expression of *ERF114* and *ERF115* for maintaining the stem cell division and differentiation balance (Kong et al., 2018). Hoermayer *et al*. demonstrated that following targeted cell death by means of laser ablation, turgor driven expansion of the adjacent cell was a prerequisite to *ERF115* activation. Furthermore, damaging of the cell wall without killing the cell was sufficient for *ERF115* induction in the presence of auxin (Hoermayer *et al.*, 2020). Similarly, treatment of intact roots with a low concentration of cell wall degrading enzymes induced *ERF114* and *ERF115* expression (Zhang et al., 2022). These data indicated a potential role for cell wall integrity signaling and acute mechanical stress in wound-induced *ERF115* activation.

One of the main drivers of plant growth and cell expansion is the dynamic interplay between intrinsic and extrinsic mechanical forces, where the direction of growth is determined by the extensibility of the cell wall. Plant cell walls are mainly made up of cellulose fibers embedded in a pectin-cellulose-hemicellulose carbohydrate matrix (Hofte and Voxeur, 2017). The extensibility of the cell wall is determined by the type and extent of crosslinks between the aforementioned components. During development the internal and external forces experienced by the cell wall are transmitted into downstream cellular signaling pathways through a variety of cell membrane localized receptors, directly linked with cell wall components. This provides the input for the cell to expand or divide, accompanied by remodeling of the cell wall to maintain homeostasis (Hofte, 2015). One of the best studied family of cell wall surveillance proteins is plant malectin-like receptor kinases, also known as CATHARANTHUS ROSEUS RECEPTOR-LIKE KINASE 1-LIKE

PROTEINS (CrRLK1Ls) (Franck et al., 2018). FERONIA (FER), a well-studied member of CrRLK1Ls family, has been shown to bind pectin *in vitro*, suggesting its association with the cell wall (Feng et al., 2018). Mutants lacking FER activity display accelerated growth, increased strain rate experienced by the root and hypersensitivity to abiotic stresses (Feng *et al.*, 2018; Shih et al., 2014). Based on these observations, FER is proposed to sense changes in the mechanical equilibrium of cell walls and negatively regulate cell wall extensibility to maintain cell wall homeostasis (Hofte, 2015). This inhibitory regulation of cell expansion contrasts with the positive regulation of cell expansion and elongation mediated by the brassinosteroid (BR) hormone signaling pathway. BR synthesis occurs locally in rapidly elongating cells and acts in a paracrine fashion through its receptor BRASSINOSTEROID INSENSITIVE 1 (BRI1) (Vukasinovic et al., 2021). The subsequent activation of transcription factor BRASSINAZOLE RESISTANT 1 (BZR1) has been shown to activate a plethora of adaptive downstream signaling cascades enriched in genes responsible for cell wall modification (Sun et al., 2010). Perturbation of cell wall integrity through pectin methyl esterase inhibition has been shown to activate BR signaling leading to adaptive changes in growth and cell wall remodeling (Wolf et al., 2012b; Wolf et al., 2014).

In this study, we demonstrate that ERF115 and its closest homolog ERF114 regulate lateral root (LR) development during regular growth likely via activation of auxin signaling. Moreover, using manual root bending, partial cell wall degradation and the *feronia* cell wall integrity receptor mutant, we demonstrate that mechanical strains contribute to *ERF114* and *ERF115* expression in both developmental and regeneration contexts by activation of BR signaling.

## Results

### ERF114 acts redundantly with ERF115 during regeneration following root tip removal

Despite being the closest homolog of *ERF115*, the importance of *ERF114* for the reconstitution of an organized root meristem following wounding has not been explored. We generated a reporter line in which the NLS-GFP/GUS fusion protein is driven by the *ERF114* promoter. Confocal imaging revelated that *ERF114* was induced strongly 5 h after removal of the distal root tip (hours post cut; hpc) and its expression diminished as a new root tip was formed at 72 hpc (Fig. 1A). Similarly, stem cell death caused by 24-h treatment with the radiomimetic drug bleomycin (BLM) evoked a strong *ERF114* and *ERF115* induction as measured by confocal microscopy and qRT-PCR (Supplementary Fig. 1A,B). Next, we created *erf114* single and *erf114 erf115* double mutants via CRISPR/Cas9-mediated mutagenesis and evaluated their ability to regenerate a *de novo* root tip 72 h after removal of the 200µm distal root tip. As previously observed (Heyman *et al.*, 2016), the dominant-negative *ERF115*$^{SRDX}$ overexpression line and *erf115* single mutants displayed a lower regeneration frequency compared to the wild type, being 1% ($p<0.001$), 31% ($p<0.001$) and 52% respectively (Fig. 1B). The regeneration frequency for *erf114* single and *erf114 erf115* double mutants were 44% ($p>0.05$) and 15% ($p<0.01$), (Fig. 1B). Taken together, these results suggested that ERF114 acts redundantly with ERF115 during root meristem regeneration.

### *ERF114* overexpression enhances sensitivity to auxin accumulation

ERF115 has previously been shown to act upstream of *MONOPTEROS* (*MP*), encoding a major regulator of various auxin-mediated developmental and regenerative processes.

(Canher *et al.*, 2020). In the absence of wounding, overexpression of *ERF115* was shown to confer sensitivity to auxin accumulation in the absence of wounding indicated by an enhanced vascular diameter as well as an expanded columella domain (Canher *et al.*, 2020). Similar to *ERF115*$^{OE}$ seedlings, after 5 days of growth on NPA or 2,4-D, *ERF114*$^{OE}$ and *ERF115*$^{OE}$ plants displayed thick roots with significantly enhanced expansion of the columella domain (Fig. 1C, Supplementary Fig. 1C). These data suggested that high levels of *ERF114* result in sensitivity to auxin accumulation, similar to ERF115.

Besides the previously reported effects on columella domain and vascular expansion, we observed that both *ERF114*$^{OE}$ and *ERF115*$^{OE}$ seedlings grown on NPA displayed ectopic xylem formation indicated by confocal images of basic fuchsin stained roots (Supplementary Fig. 1D). In contrast to the absence of differentiated xylem cell files in wild-type roots, both *ERF114*$^{OE}$ and *ERF115*$^{OE}$ seedlings displayed multiple xylem strands at 200-250µM from the root tips (Fig. S2A). While these data suggest a similar functionality between *ERF114* and *ERF115* during regeneration, long-term NPA treatment revealed potential differences in functionality. Growth in the presence of NPA has been found to inhibit LR primordium (LRP) formation and outgrowth, due to the essential role of polar auxin transport in the formation of lateral organs (Casimiro et al., 2001). In accordance with these reports, 14-day-old wild-type seedlings grown on 10 µM NPA produced no LRs (Supplementary Fig. 2B). Surprisingly, *ERF114*$^{OE}$ seedlings grown on NPA displayed developed LRs whereas no LRPs were observed in *ERF115*$^{OE}$ seedlings (Supplementary Fig. 2B). demonstrating that high *ERF114* levels allow to initiate lateral roots regardless of auxin transport inhibition.

**Both ERF114 and ERF115 are part of the developmental LR formation program**

ERF115 has been shown to act as an activator of *MP*, a master regulator for a plethora of auxin mediated LR formation (Bhatia *et al.*, 2016; Canher *et al.*, 2020; De Smet, 2010; Przemeck *et al.*, 1996). Due to the formation of LRs on NPA-treated *ERF114$^{OE}$* seedlings, we investigated if *ERF114* and *ERF115* might be involved in LR formation under control conditions. Given the observed auxin hypersensitivity phenotypes, *MP:MP-GFP* was crossed with *ERF114$^{OE}$*, *ERF115$^{OE}$* and Col-0 followed by quantification of MP-GFP signal from confocal images. In primary root meristems, average MP-GFP intensity was significantly higher in *ERF114$^{OE}$* and *ERF115$^{OE}$* compared to wild type, especially in the 80-120um region ($p<0.01$) from the root tip, which corresponded to the stem cell niche (Fig. 1D,E). Furthermore, *ERF114* overexpression resulted in significantly increased average GFP intensity in stage II LR primordia compared to LRs of control plants of the same stage (Fig. 2A,B). Whereas *ERF115* overexpression also resulted in an increase, the difference was not statistically significant. Overall, these results suggested that increased levels of *ERF114* and *ERF115* can result in accumulation of MP in LRs or primary root meristems.

*DR5:LUCIFERASE* (*DR5:LUC*) reporter is commonly used to visualize the LRP sites marked by auxin maxima (Moreno-Risueno et al., 2010). To examine if *ERF114* and *ERF115* control LRP initiation, we crossed the *DR5:LUC* reporter with the *ERF115$^{OE}$* and *ERF115$^{SRDX}$* overexpression lines and acquired luciferase luminescence images in the F1 generation. (Fig. 2C,D). LRP densities were also determined from differential interference contrast images after clearing as previously described (Malamy, 1997).

*ERF115*$^{OE}$ and *ERF115*$^{SRDX}$ hemizygous seedlings showed respectively a significantly increased and decreased number of LRPs, whereas root lengths were significantly lower compared to wild type (Supplementary Fig. 2C). The number of LRPs per cm of root (indicated as LRP density, Fig. 2E) and number of *DR5:LUCmax* per cm of root (indicated as *DR5:LUCmax* density, Fig. 2F) were significantly higher in *ERF115*$^{OE}$ and lower in *ERF115*$^{SRDX}$ compared to wild type. Similarly to *ERF115*$^{OE}$, *ERF114*$^{OE}$ seedlings had increased LRP and *DR5:LUC* maxima densities (Fig. 2G,H) while having similar average root length compared to wild type (Supplementary Fig 2E). To confirm the involvement of *ERF115* in the production of auxin maxima, we rotated the plates on which the *DR5:LUC ERF115*$^{SRDX}$ seedlings were growing for 90$^{o}$, a process known to induce a gravitropic curvature in the roots accompanied by the accumulation of auxin at the bend site (Lucas et al., 2008). Luminescence time-lapse imaging after 90$^{o}$ rotation indicated that a significantly reduced number of auxin maxima formed at the bend site of *DR5:LUC ERF115*$^{SRDX}$ roots compared to the wild type (Supplementary Fig. 2D), further suggesting the involvement of ERF115 in the formation of bending-induced auxin maxima.

Next, we investigated how *ERF114* and *ERF115* loss of function would impact LR development. To this end, we introduced the *DR5:LUC* reporter into *erf114* and *erf115* single and *erf114 erf115* double backgrounds. We noticed that the *erf114* and *erf115* single mutants and the *erf114 erf115* double mutants displayed a significantly reduced LR density compared to wild-type plants (Fig. 3A). Luminescence imaging of *DR5:LUC* showed that *erf115* single and *erf114 erf115* double mutants displayed a significant reduction in *DR5:LUC* maxima density compared to the wild type (Fig. 3B). The *erf114* single mutant also showed a reduced *DR5:LUC* maxima density but the difference was

not statistically significant. The average root lengths of mutants were not significantly different compared to wild type (Supplementary Fig. 2F). To determine the contribution of *ERF114* and *ERF115* to the amplitude of the auxin signaling, average *DR5:LUC* signal intensity plotted over 0.3cm region of the root tip containing the meristematic zone (MZ) and oscillation zone (OZ) (Fig. 3C,D). Average *DR5:LUC* signal intensity in *erf114* and *erf115* single mutants were not significantly different than wild type. However, the *erf114 erf115* double mutant showed a significant difference ($F<0.001$) compared to wild-type with a clear reduction in the 0.1cm region that corresponds to the MZ. This suggested that *ERF114* and *ERF115* also contributes to the intensity of the auxin signaling.

To determine the putative contributions of *ERF114* and *ERF115* to the overall root system architecture, we obtained scanned images from 13day old roots and quantified traits using RootNav (Pound et al., 2013) (Supplementary Fig. 3A). Among the 7 traits analyzed, the number of LRs had the greatest variation with $ERF114^{OE}$ having the highest (8.2 ± 0.6, $p<0.06$) and $ERF115^{SRDX}$ having the lowest (1.1 ± 0.5, $p<0.05$) number of LRs compared to wild-type (4.7 ± 0.5) (Supplementary Fig.3 B,C). The increased number of LRs in the $ERF114^{OE}$ line was accompanied by a significant decrease in LR emergence angle (33.1 ± 2.6º vs 47 ± 2.4º, $p<0.05$) and primary root length (4.7 ± 0.2cm vs 5.1 ± 0.12cm, $p<0.05$) compared to wild-type. The $ERF115^{OE}$ line also showed a significant decrease in primary root length (4.42 ± 0.14cm, $p<0.05$) accompanied by a similar increase in number of LRs (5.74 ± 0.62) and decrease in LR emergence angle (41.1 ± 1.6º) but differences were not statistically significant. The *erf114*, *erf115* and *erf114 erf115* mutant lines showed a decrease in the number of LRs compared to wild-type (4.2 ± 0.68, 3.6 ± 0.49, 4.2 ± 0.48 vs 5,2 ± 0.7, respectively), even though the differences were not statistically significant.

This is likely due to the relatively small number of LRs being outgrown at the time of analysis and the absence of a specific effect in the LR emergence (Fig. 3A). These results suggested contribution of *ERF114* and *ERF115* towards LR formation within first 2 weeks of growth is largely at the level of LR production.

Taken together, these data suggest that next to wound induced regeneration, both *ERF114* and *ERF115* promote LR formation through activation of auxin signaling. This activation is likely results from positive regulation of MP, considering its induction upon *ERF114* or *ERF115* overexpression.

**Spatial-temporal control of *ERF114* and *ERF115* expression reveals correlation between protoxylem maturation and LR initiation**

Despite the data indicating a role for ERF114 and ERF115 in the process of LR development, expression of these transcription factor genes in LR primordia has thus far not been reported, which prompted us to investigate potential LR-specific *ERF114* and *ERF115* expression in detail. Confocal imaging of *pERF115:NLS-GFP/GUS* seedlings, grown under control conditions, showed a relatively weak (requiring high laser power) and sporadic expression of *ERF115* in protoxylem cells (Fig. 3E), in line with a previous study (Zhou *et al.*, 2019). *PASPA3* expression has been shown to mark maturing protoxylem cells undergoing programmed cell death (Fendrych et al., 2014). Time-lapse imaging of a *pPASPA3:tdTOMATO-NLS pERF115:NLS-GFP/GUS* dual reporter line showed that *ERF115* expression overlapped with that of *PASPA*3, suggesting that *ERF115* expression correlates with the maturation of protoxylem cells (Supplementary Fig. 4A, Supplementary Movie 1). The sudden disappearance of both fluorescent signals

in the older protoxylem cells (as indicated by the disappearance of arrows in Supplementary Fig. 4A and Supplementary Movie 1) likely results from nuclear disintegration in the last stages of programmed cell death. However, no *ERF115* expression could be detected in LRP. To investigate if *ERF115* expression was also lacking in uninitiated LRs named prebranch sites, we introduced the *DR5:RFP* reporter, which is activated prior to LR initiation (Moller et al., 2017), into the *ERF115* reporter line. Time-lapse imaging using the *pERF115:GFP-NLS pDR5:RFP* dual reporter line confirmed that the prebranch sites marked by the *DR5:RFP* signal did not harbor a detectable *ERF115:GFP-NLS* signal (Supplementary Movie 2. Supplementary Fig. 4B). However, we noticed that the *ERF115:GFP-NLS* signal in the protoxylem (nuclei marked by white arrowhead at t=09:12) had a tendency to disappear shortly after the *DR5:RFP* signal started accumulating in the LR founder cells (marked by blue arrowhead at t=08:37), which subsequently forms the LRP (Supplementary Movie 2). To investigate this correlation in more detail, time-lapse imaging was performed after rotating the seedlings 90$^{o}$C to synchronously induce LR formation. The *DR5:RFP* signal appeared in the founder cell 1.6 ± 0.7 h (n=6) before the disappearance of the *ERF115:GFP-NLS* signal in the adjacent protoxylem, suggesting a temporal correlation. Likewise, *pDR5:VENUS-NLS pPASPA3:tdTOMATO-NLS* time-lapse imaging revealed that the *DR5:VENUS-NLS* signal in the founder cell appeared on average 1.1 ± 0.5 h (n=7) before the *pPASPA3:tdTomato-NLS* signal disappeared in the adjacent protoxylem (Supplementary Movie 3, Supplementary Fig. 4C). These results suggest that whereas *ERF115* is not expressed in the LR founder cell, there is a temporal correlation between

the activation of auxin signaling in the founder cell and the nuclear degradation of adjacent protoxylem cells expressing *ERF115*.

Differently from *ERF115*, expression of *ERF114* could be detected in pericycle cells while being absent in the protoxylem (Fig. 3F,G). Time lapse confocal imaging indicated that pericycles cells carrying an ERF114:GFP signal formed a LR primordia (Supplementary Fig. 5A). Expression of *ERF114* in the pericycle was accompanied by a *DR5:RFP* signal, which marks the LR founder cell prior to initiation (Fig. 3G, Supplementary Fig. 5B). *ERF114* expression in the founder cell preceded the first appearance of the *DR5:RFP* signal by 1.4 ± 1.1 h (n=6) (Supplementary Movie 4, Supplementary Fig. 5B). Similarly, *ERF114* expression in the founder cell preceded the protoxylem cell death by 2.75 ± 0.5 h (n=6).

**Cell wall damage, mechanical stress and endodermal cell removal induce *ERF114* expression**

Hoermayer *et al*. recently demonstrated that following laser-assisted cell ablation, cell expansion is necessary for the induction of *ERF115*. Moreover, damaging the cell wall without causing cell death in the presence of auxin was sufficient for robust induction of *ERF115* (Hoermayer *et al.*, 2020). Based on these observations, we hypothesized that the expression of *ERF114* and *ERF115* during the process of LR formation might be influenced by mechanosensitive cues or cell wall stresses. To test this hypothesis, we damaged the cell wall at the intersection of two immature protoxylem cells using low-intensity laser exposure without causing cell death, as indicated by lack of intense PI staining (red) (Fig. 4A). Protoxylem ablation in the *pERF114:GFP-NLS/GUS* background

was followed by rapid induction (5.5 and 8 hours post ablation (hpa)) of *ERF114* in the adjacent pericycle cells, suggesting that cell wall damage signals coming from the neighboring protoxylem induces pericycle-specific *ERF114* expression (Fig. 4A, Supplementary Movie 5). Previously, it has been proposed that endodermal cells act as inhibitors of LR development and that laser-assisted endodermal cell ablation (ECA) triggers periclinal divisions in the underlying pericycle cells. Mutants impaired in auxin signaling and transport still display periclinal divisions upon ECA, albeit in a reduced frequency, hinting towards the involvement of additional processes independent of auxin signaling (Marhavy et al., 2016). To check whether *ERF114* might be involved in this process, we performed ECA using a high laser intensity. ECA triggered strong *ERF114* induction in the pericycle followed by periclinal and anticlinal divisions in the surrounding pericycle cells (Fig. 4B). While it is tempting to speculate about a potential causative link between *ERF114* and *ERF115* expression and naturally occurring protoxylem and/or endodermal cell death and, maturation of the protoxylem has not been found to be necessary for LR initiation (Parizot et al., 2008). Therefore, it is unlikely that the cell death itself is triggering *ERF114* and *ERF115* expression in LR founder cells and the protoxylem, respectively. Transient mechanical bending of roots has been shown to be sufficient to induce an LR even in mutants with severely impaired auxin signaling such as *tir-1* and *arf7 ar19* (Ditengou et al., 2008). Furthermore, LRs have been shown to be located at the sites of curvature resulting from auxin-dependent root waving (De Smet et al., 2007). Therefore, we hypothesized that instead of the cell death, the localized mechanical strains associated with natural curvature of the root growth might be developmental triggers for *ERF114* and *ERF115*. To test this hypothesis, we applied

mechanical stress by manual bending the root tip and releasing it, as described previously (Ditengou *et al.*, 2008). Absence of intense PI staining (cyan) suggested that no cell death occurred during the process (Fig. 4C, Supplementary Movie 6). Manual root bending triggered strong *ERF114* expression in multiple pericycle cells along the bent region, followed by LR primordia initiation in a subset of *ERF114* positive cells carrying a strong *DR5:RFP* signal (Fig. 6C, Supplementary Movie 6). Similarly, manual bending also caused rapid induction of *ERF115* but in tissues underlying the LR primordia carrying the *DR5:RFP* signal (Supplementary Movie 7). To quantify the *ERF114* induction, we acquired confocal images from *pERF114:NLS-GFP/GUS* seedlings after manual bending (Fig 4D). For comparison, roots were not bent but the position at which they would have been bent were marked on the agar plate. Control roots (indicated as “not-bent”) were imaged at the marked position along with the bent roots and total GFP signal was quantified as mean gray value. Manual bending triggered a strong increase in GFP mean gray value (0.3 in control vs 10.1 in bent roots, $p<0.001$) (Fig. 4E).

Pectinase and cellulase treatments were recently shown to activate *ERF115* in hypocotyls during grafting as well as primary roots (Zhang *et al.*, 2022). Therefore, to independently test the involvement of cell wall damage in activation of *ERF114* in LRPs, we treated *pERF114:NLS-GFP/GUS* seedlings with a low concentration (0.003%) of macerozyme, a commonly used pectinase enzyme that results in cell wall degradation by cleavage of interlinked pectin (Koziol et al., 2017). GFP quantification based on confocal images of stage II LRPs revealed a significant induction (mean gray values of 22.6 in control vs 46.6 in treated roots, $p<0.05$) upon macerozyme treatment (Fig. 4F,G). Taken together these

data demonstrate that mechanical stress is sufficient to trigger *ERF114* expression and partial cell wall degradation can enhance its expression in LRPs.

**The cell wall-associated mechanosensor FERONIA receptor kinase limits developmental and wound-induced *ERF114* and *ERF115* expression**

Cell wall damage signaling has been reported to activate BR hormone signaling that in turn modifies the cell wall architecture to increase cell wall extensibility (Wolf *et al.*, 2012b). Following DNA damage-induced stem cell death caused by BLM, cell expansion of neighboring cells has been shown to be necessary for *ERF115* activation (Hoermayer *et al.*, 2020). Since BZR1, one of the main transducers of BR signaling was shown to bind directly to the *ERF115* promoter, and BL treatment enhanced *ERF115* expression levels (Chaiwanon and Wang, 2015; Heyman *et al.*, 2013; Lee et al., 2015; Wang et al., 2002), we tested if BZR1 expression is activated upon BLM treatment in expanding cells neighboring the dead ones. Confocal imaging of the BR signaling reporter *pBZR1:BZR1-GFP* suggested that BLM-induced stem cell death results in an accumulation of BZR1 around the dead cells (Fig. 5A), in agreement with the previously reported activation of wound-induced BR signaling (Wolf et al., 2012a). We reasoned that activation of BZR1 during the LR formation could be indicative of perceived cell wall stress. Time-lapse imaging using the *pBZR1:BZR1-GFP* reporter line showed accumulation of BZR1 in pericycle cells that undergo typical anticlinal divisions during LRP initiation (Supplementary Movie 8). Time lapse imaging of a *pBZR1:BZR1-GFP DR5:RFP* dual reporter line suggested a similar BZR1 accumulation (marked by white arrow heads) in the LR founder cells (12hpr) and initiated primordia, as marked by *DR5:RFP* accumulation (14h-24hpr) (Fig. 5B). To determine the contribution of BR signaling in *ERF114* activation

upon mechanical bending, we introduced the *pERF114:NLS-GFP/GUS* reporter into *comfortably numb 1* (*cnu1*) background, a *BRASSINOSTEROID INSENSITIVE 1 (BRI1)* loss of function mutant (Wolf *et al.*, 2012a). Manual root bending was performed on *pERF114:NLS-GFP/GUS* seedlings in wild-type or *cnu1* mutant background, followed by confocal imaging. In the non-bent group, 34% of wild-type and 36% of *cnu1* roots had one LRP formed at the marked region, whereas the remainder had no LRPs. Among the bent group, nearly all wild type roots displayed one LRP (47%) or two LRPs (50%) at the bent region while only 3% displayed zero LRP. In the *cnu1* background, the proportion or roots with one LRP (70%) or two LRPs (19%) were significantly different compared to wild-type whereas 11% had zero LRP ($p<0.05$) (Fig. 5C). Furthermore, quantification of the GFP signal from roots with only one LRP revealed a significant reduction in *ERF114* expression in the *cnu1* background, compared to wild-type (3.5 vs 13.6, $p<0.001$) (Fig. 5D,E). Taken together, these results suggested that BR signaling is involved in induction of *ERF114* and formation of LRPs upon mechanical stress.

While activation of BR signaling (via *BZR1*) during regular LR formation suggested the possibility of a perceived mechanical or cell wall stress during development, it cannot rule out the involvement of non-stress related processes activating *BZR1*. To address this shortcoming, we utilized a reverse genetics approach. It was previously suggested that FERONIA (FER), a member of RECEPTOR LIKE KINASE (RLK) family, works antagonistically to the BR signaling and negatively regulates cell extensibility (Hofte, 2015). FER has been shown to sense growth-related mechanical stress and activate compensatory, growth-limiting pathways. The loss of function mutant *fer-4* was characterized by an increased strain in the root elongation zone and an accelerated

development of LRs (Shih *et al.*, 2014). Therefore, we hypothesized that if a growth-related mechanical strain controls the activation of *ERF114* and *ERF115* expression, *fer-4* mutant seedlings might display increased levels of *ERF114* and *ERF115*. Indeed, the expression levels of both *ERF114* and *ERF115* were significantly increased in the 1-cm distal root tip section of *fer-4* mutants, compared to the wild type (Fig. 5F). To confirm this observation, we introduced the *ERF114* and *ERF115* transcriptional reporter lines into the *fer-4* background. Hyperactivation of *ERF114* and *ERF115* was clearly visible in aerial tissues, as indicated by intense GUS staining at the cotyledon-hypocotyl intersection (Fig. 6A). In the roots, *ERF115* expression was strongly enhanced mainly in the protoxylem cell file (Fig. 5G). *ERF114* expression was also substantially increased in the pericycle cells and LR primordia (Fig. 5G,H). This coincided with a significantly increased LRP density in *fer-4* seedlings compared to the wild type (Fig. 5I). Treatment with auxin resulted in a visibly stronger induction of both *ERF114* and *ERF115* in the roots of the *fer-4* background compared to the wild type (Fig. 6B,C), suggesting that FER might negatively regulate the auxin responsiveness of *ERF114* and *ERF115* expression.

Next, we investigated if FER might also restrain wound-induced *ERF115* expression, which was previously demonstrated to be accompanied by auxin accumulation (Canher *et al.*, 2020). Induction of stem cell death after a 24-h treatment of *pERF115:GFP-NLS/GUS* seedlings with BLM resulted in an enhanced induction of *ERF115* in the *fer-4* background (Fig. 5J). Quantification of GFP integrity density from confocal images revealed a 74% increase ($p<0,001$) in *fer-4* compared to the wild type (Fig. 5K,L). Taken together, these results suggest that developmental and wound-specific *ERF114* and *ERF115* expression might be influenced by growth-related mechanical cues, with FER-

dependent cell wall signaling negatively regulating auxin sensitivity in a tissue-specific manner.

## Discussion

### A developmental role for *ERF114* and *ERF115* in LR formation

*ERF114* and *ERF115* have been the focus of extensive research regarding wound response and regeneration. In this study, we demonstrated that ERF115 and ERF114 act redundantly during meristem regeneration following wounding (Fig 1B, Supplementary Table 1). *ERF115* was recently shown to be induced upon hypocotyl cutting and in parallel with an accumulation of auxin, to promote graft formation (Melnyk et al., 2018; Zhang *et al.*, 2022) (Supplementary Fig. 1E,F). High *ERF114* and *ERF115* transcript levels are also associated with ectopic xylem formation (Fig. 1C, Supplementary Fig. 1D) that is essential for establishing xylem reconnection during hypocotyl grafting. We show that *erf114 erf115* mutants display significantly reduced xylem reconnection between rootstock and scion as revealed by grafting assays (Supplementary Fig. 1E,F). While these results point towards involvement or *ERF114* and *ERF115* xylem formation, further research will be required to determine if these are distinct from their established roles in regeneration.

However, presumably due to their low expression levels, involvement of *ERF114* and *ERF115* in a developmental context has not been explored besides regulation of QC cell divisions (Heyman *et al.*, 2013). Here, we showed that *ERF114* and *ERF115* activate auxin signaling at least via induction of *MP* (Figs. 1D,E and 2A-D) and promote LR development (Fig. 2C-H). Even though *ERF115* expression could only be detected in protoxylem (Fig. 3E, Supplementary Movies 1 and 2), *erf115* mutants displayed a reduced

LR formation (Fig. 3B) and auxin maxima density (Fig. 3A, Supplementary Table 1). Smetana *et al*. showed that during secondary growth, immature xylem cells carrying local auxin maxima act non-cell autonomously as organizer cells. Clonal activation of auxin signaling via MP was sufficient to trigger xylem vessel differentiation and subsequent formative divisions in the adjacent procambial and pericycle cells (Smetana et al., 2019). Previously, misexpression of *ERF115* in the endodermis, in combination with auxin accumulation, was shown to non-cell autonomously produce formative divisions in columella stem cells (Canher *et al.*, 2020). Therefore, based on its protoxylem-specific expression and being an upstream inducer of *MP*, ERF115 might act non-cell autonomously on the adjacent pericycle cells carrying an auxin maximum to grant stem cell identity to founder cells.

Differently, *ERF114* expression is detected in LR founder cells (Fig. 3G, Supplementary Fig. 4A,B) and its overexpression, unlike *ERF115*, led to the formation of LRs in the presence of NPA (Fig. 2B). Interestingly, the *ERF114*$^{OE}$ line has higher levels of MP in the LRPs compared to *ERF115*$^{OE}$ despite having lower MP levels in the primary roots. Therefore, phenotypic differences between *ERF114*$^{OE}$ and *ERF115*$^{OE}$ lines could be due to differential activation of MP on a tissue specific level. However, we cannot rule out the possibility that these differences are caused by differences in overexpression levels. Mehrnia *et al*. previously described *ERF114* as an inducer of axillary bud formation and outgrowth, where *Pectin Methyl Esterase Super Family Protein* (At3g62820), auxin influx carrier *AUXIN RESISTANT 1* and *CYCLIN D3;3* were among the induced genes in an *ERF114*-inducible overexpression system (Mehrnia *et al.*, 2013). Cell wall softening using external pectin methyl esterase application was sufficient to result in lateral organ

initiation in auxin transport-deficient *pin1* mutants (Braybrook and Peaucelle, 2013). Thus, it is plausible that different downstream targets of *ERF114* and *ERF115* contribute to the phenotypic differences. Taken together with the differences in tissues where *ERF114* and *ERF115* are expressed, these data suggest that they might serve overlapping but not identical functions during LR formation and development.

**_ERF114_ and _ERF115_ expression during growth and regeneration is driven by mechanical cues and regulated antagonistically by FER and BR signaling**

Time-lapse confocal imaging revealed a series of events displaying a spatial-temporal correlation, starting with *ERF114* induction in the LR founder cell, followed by DR5 activation in the founder cell (Supplementary Fig.5, Supplementary Movie 4) and ending with the programmed cell death (Supplementary Fig. 4C, Supplementary Movie 3) of the adjacent protoxylem cell expressing *ERF115* (Supplementary Fig. 4B, Supplementary Movie 1). We show that mechanical bending is sufficient to induce *ERF114* (Fig. 4D,E). Moreover, *fer-4* mutants, which are associated with an increased maximal strain and LR density, displayed a strong activation of both *ERF114* and *ERF115* (Fig. 5F-H, Fig. 6A, Supplementary Table 1) (Dong et al., 2019). Application of auxin resulted in an additional hyperactivation of *ERF114* and *ERF115* in *fer-4* seedlings (Fig. 6B,C). Our results support a framework in which mechanical cues drive the expression of *ERF114* and *ERF115* during both regeneration and development. (Fig. 7). In this framework, cell wall integrity and mechanosensory FERONIA-mediated signaling constitutes a feedback mechanism that negatively regulate the expression of *ERF114* and *ERF115* in LR and xylem cells, respectively. In the absence of wounding, developmentally driven mechanical pressures contribute to *ERF114* and *ERF115* expression. Subsequent activation of MP-mediated

auxin signaling by *ERF115* and *ERF114* in turn likely drives LR development. While activation of *ERF114* by mechanical strain promotes LR progression and outgrowth, the exact downstream targets potentially unique to ERF114 are yet to be identified. In the context of regeneration, similar cell wall damage or cell death induced pressure changes activate *ERF115* and *ERF114*. Like the developmental context, this is followed by activation of MP mediated auxin signaling which enables regeneration.

The upstream receptor mechanisms and chemical changes that act upstream of *ERF114* and *ERF115* upon mechanical cues still need to be investigated. RAPID ALKALINIZATION FACTOR 1 (RALF1) is a secreted ligand of FER and has been shown to inhibit cell elongation and LR formation by antagonizing BR signaling (Bergonci et al., 2014; Yu et al., 2020). Furthermore, it has recently been suggested that mechanical bending, wounding or treatment results in a decrease in FER abundance in the plasma membrane (Cornblatt et al., 2021). Therefore, it can be speculated that activation of FER signaling through RALF1 could maintain repression of *ERF114* in the absence of mechanical strain of cell wall cues. It will be of interest to determine if FER downregulation occurs after wounding, similar to that observed after mechanical bending. Next to FERONIA, a number of CWI sensors associated with mechano-perception such as members of the MECHANOSENSITIVE CHANNEL OF SMALL CONDUCTANCE LIKE (MSL) and MID1-COMPLEMENTING ACTIVITY A (MCA) gene families are prime candidates as upstream regulators of *ERF114* and *ERF115* (Bacete and Hamann, 2020). Additionally, RECEPTOR LIKE PROTEIN 44 (RLP44), a cell wall integrity sensor which shown to mediate the activation of BR signaling in response to cell wall damage, stands out as a putative upstream regulator (Wolf *et al.*, 2014). Interestingly, *RLP44* was

demonstrated to regulate phytosulfokine signaling through its interaction partner PHYTOSULFOKINE RECEPTOR 1 (PSKR1) and prevent xylem fate acquirement in the cambium (Holzwart et al., 2018). Considering that ERF115 is a direct activator of *PSK5*, RLP44 is worth investigation as a wall integrity sensor activating *ERF115* and *PSK5* expression during development and regeneration.

## Methods

### Plant materials and growth conditions

Plants were grown under a long-day regime (16-h light/8-h darkness) on agar-solidified culture medium (Murashige and Skoog [MS] medium, 10 g/l saccharose, 4.3 g/l 2-(N-morpholino) ethanesulfonic acid [MES], and 0.8% plant tissue culture agar) at 21°C. *MP:MP-GFP* seeds were kindly provided by Dolf Weijers, Wageningen University, Netherlands (Cole et al., 2009; Schlereth et al., 2010). *pPASPA3:tdTomato-NLS* (Xuan et al., 2016), *DR5:LUC* (Moreno-Risueno *et al.*, 2010), $ERF115^{OE}$, $ERF115^{SRDX}$, *pERF115:NLS-GFP/GUS* and *erf115* (SALK_021981) were described previously (Heyman *et al.*, 2013). The $ERF114^{OE}$ construct was made by inserting *ERF114* (AT5G61890) CDS in to pK2GW7 (Karimi et al., 2002) destination vector, carrying *35S* promoter, via gateway cloning. The *pERF114-NLS-GFP/GUS* reporter was created by cloning the 2163 nucleotide promoter region upstream of *ERF114* start codon into the pCR™Blunt II-TOPO® vector. The resulting entry vector was cloned into pMK7S*NFm14GW (Karimi *et al.*, 2002). Obtained expression constructs were transformed into the Col-0 background by agrobacterium-mediated transformation. The

*ERF114* CRISPR mutant (Supplementary Fig. 6) was created using a dual guide RNA approach (Pauwels et al., 2018). A construct targeting two different sites in the *ERF114* gene was designed where the single guide RNA1 (sgRNA1, pMR217_pDONR_P1P) and sgRNA2 (pMR218_pDONR_P5P) were annealed and inserted via a cut ligation method using Bbs1 in pMR217_pDONR_P1P and pMR218_pDONR_P5P, respectively. Next, using a Gateway LR reaction the two sgRNAs were combined into pDE_CAS9_Basta to yield the final expression clone. The *erf114 115* double mutants (Supplementary Fig. 6) were obtained by transforming the *ERF11*4 CRSIPR construct into the *erf115* single mutant by floral dip method. Primary transformants were selected on agar plates containing Basta and genotyped for the deleted fragment and further confirmed using Sanger sequencing. Cas9 free and homozygous mutants were selected in the T3 generation for further use. Primers used for the CRISPR-mediated mutagenesis and genotyping are described in Supplementary Table 2.

**Lateral root staging**

Eight-day-old seedlings were fixed in 80% acetone overnight. After discarding the acetone, seedlings were treated with Clearsee optical clearing solution overnight to increase transparency of tissues (Kurihara et al., 2015). The next day, Clearsee solution was discarded, and seedlings were rinsed with distilled water to wash off the remaining Clearsee solution. Further clearing and staging was performed as described previously, starting with the acid clearing step (Malamy, 1997). The counting of the LRs was done using an Olympus BX51 DIC microscope.

**DR5:LUC imaging**

A Lumazone imaging system equipped with a charge-coupled device (CCD) camera (Princeton Instruments, Trenton, NJ, USA) was used for luciferase imaging. The CCD camera is controlled by WinView/32 software. For imaging DR5:LUC expression, square plates containing ½ MS medium with or without chemicals were sprayed with 1-mM D-Luciferin solution (0.01% Tween80) and left to dry in the dark. Eight-day-old DR5:LUC seedlings were transferred onto the plates and imaged immediately with a macro lens with a 20-min exposure time for indicated time points. For time-lapse imaging, an image was acquired every 20 min. The picture series were saved as TIFF format by WinView/32 software for further analysis in ImageJ (http://imagej.nih.gov/ij/). The prebranch site densities were calculated by dividing the number of DR5 maxima by the root length. The gravitational bending assay was done by rotating the square plate holding the seedlings 90° and imaging the *DR5:LUC* overnight with 30-min intervals. Number of *DR5:LUC* maxima at the bend site was calculated from the obtained time-lapse imaging.

**GFP signal Quantification from Confocal Images**

For MP-GFP signal quantification in primary root meristems confocal images (Fig. 4A) were converted to 8-bit, a manual threshold (MinGray=5,MaxGray=255) was set and mean gray values were obtained using Plot Profile function in ImageJ. Mean gray values were summed for each 10µM section and plotted with respect to their distance to the root tip (Fig. 4B). For MP-GFP signal quantification in stage II LRPs, mean gray value in a manually defined ROI (50x300pixels) that contained only the LRP cells was measured following 8-bit conversion and thresholding. GFP signal (Fig. 4F,G) from macerozyme and mock treated *pERF114:NLS-GFP/GUS* stage II LRPs were quantified similarly with

a different threshold (MinGray=20, MaxGray=255). GFP signal (Fig. 4D,E) from manually bent *pERF114:NLS-GFP/GUS* roots were quantified as mean gray value from entire confocal image with an adjusted threshold (MinGray=12, MaxGray=255).

**Histochemical assays**

β-glucuronidase (GUS) staining was performed as described previously (Lammens et al., 2008).

**Quantitative RT-PCR**

RNA was isolated from the respective tissues with the RNeasy isolation kit (Qiagen). DNase treatment with the RQ1 RNase-Free DNase (Promega) was performed before cDNA synthesis with the iScript cDNA Synthesis Kit (Bio-Rad). Relative expression levels were determined by qRT-PCR with the LightCycler 480 Real-Time SYBR Green PCR System (Roche). The primers used are described in Supplementary Table 3. The *RPS26C* and *EMB238*6 reference genes were used for normalization. In three biological repetitions, total RNA was isolated by means of the RNeasy Plant mini kit (Qiagen). For the root tips, seedlings were sown and grown for 5 days on nylon meshes (Prosep) and subsequently harvested using a scalpel. Quantitative PCR data were analyzed using the 2(–ΔΔCt) method.

**Statistical analysis**

Statistical analysis was performed using SAS Enterprise Guide 7.15 HF8. For LR quantifications, the mixed model procedure was used to calculate significance values for pairwise comparisons with the wild type by least squares post-hoc tests and corrected for multiple testing using the Bonferroni Method. Genotype was added as a main effect and

experimental repeats were included as random effect. Degrees of freedom were calculated by the Kenward-Rogers method. For regeneration assays probabilities of successful regeneration were compared using logistic regression analysis on binomial outcome data and two-sided T-tests. P-values were corrected for multiple testing by Bonferroni method. Analysis were performed using Genstat v21 (VSN International (2021), Hemel Hempstead, UK). For the comparison of MP-GFP mean gray values in primary meristems (Fig 4B), a linear mixed model of the following form (random terms underlined): response = μ + genotype + region + genotype.region + root.region was fitted to the MeanGray data, using the residual maximum likelihood (REML) approach as implemented in Genstat v21. The interaction term root.region represents the residual error term with dependent errors because the measurements are taken on the same root, causing spatial correlations among observations within roots. The autoregressive correlation structure (AR1) was selected as best correlation model to account for the spatial correlation between measurements within roots. Regions of measurement were set at equal intervals. Significances of the fixed main effects, two-way interaction terms and pairwise comparisons between genotype effects across regions and at each single region, were assessed by a modified F-test. Same model and criteria were used for the statistical comparison of *DR5:LUC* intensity in the root tips (Fig. 3C),

**Regeneration assays**

Grafting was performed as described previously and xylem connectivity was determined by CFDA fluorescence in the cotyledons (Melnyk, 2017). For assessment of xylem bridge formation in LRs, 3-day-old seedlings were rotated 90° to synchronously induce LRs.

Stringent root tip cutting was performed at a 250-µM distance from the root tip, as described previously (Sena et al., 2009).

**Treatments**

For germination for the NPA experiments, 125mM NPA stock in DMSO was diluted to a final concentration of 10 µM in ½ MS agar medium. Seedlings were germinated and grown on NPA medium for indicated times, stained with Lugol solution and imaged by light microscopy. Basic Fuchsin staining in combination with Clearsee was performed as described previously (Ursache et al., 2018). For BLM treatments, 5-day-old seedlings were transferred to medium supplemented with 0.6 mg/L bleomycin sulphate (Calbiochem) for 24 h.

**Confocal and light microscopy**

Arabidopsis roots were stained using PI by incubation in a 10-µM solution for 3 min before imaging. Imaging and laser ablation was performed on a Leica TCS SP8 X microscope equipped with an Argon laser (488 nm) for GFP excitation and a white light laser (554 nm) for tdTomato excitation. GFP and tdTomato emissions were collected at 500-540 nm and 570-630 nm, respectively. Time-lapse imaging was performed by acquiring multiple z-slice images of seedlings mounted in live imaging chambers every 30 min. Manual root bending was performed as described previously (Ditengou *et al.*, 2008). Leica LAS X and Fiji were used for further image processing. For light and differential interference contrast microscopy, an Olympus BX51 microscope was used.

## References

**Bacete, L., and Hamann, T.** (2020). The Role of Mechanoperception in Plant Cell Wall Integrity Maintenance. Plants (Basel) **9**10.3390/plants9050574.

**Bergonci, T., Ribeiro, B., Ceciliato, P.H., Guerrero-Abad, J.C., Silva-Filho, M.C., and Moura, D.S.** (2014). Arabidopsis thaliana RALF1 opposes brassinosteroid effects on root cell elongation and lateral root formation. J Exp Bot **65**:2219-2230. 10.1093/jxb/eru099.

**Bhatia, N., Bozorg, B., Larsson, A., Ohno, C., Jonsson, H., and Heisler, M.G.** (2016). Auxin Acts through MONOPTEROS to Regulate Plant Cell Polarity and Pattern Phyllotaxis. Curr Biol **26**:3202-3208. 10.1016/j.cub.2016.09.044.

**Birnbaum, K.D., and Sanchez Alvarado, A.** (2008). Slicing across kingdoms: regeneration in plants and animals. Cell **132**:697-710. 10.1016/j.cell.2008.01.040.

**Braybrook, S.A., and Peaucelle, A.** (2013). Mechano-chemical aspects of organ formation in Arabidopsis thaliana: the relationship between auxin and pectin. PLoS One **8**:e57813. 10.1371/journal.pone.0057813.

**Cai, X.T., Xu, P., Zhao, P.X., Liu, R., Yu, L.H., and Xiang, C.B.** (2014). Arabidopsis ERF109 mediates cross-talk between jasmonic acid and auxin biosynthesis during lateral root formation. Nat Commun **5**:5833. 10.1038/ncomms6833.

**Canher, B., Heyman, J., Savina, M., Devendran, A., Eekhout, T., Vercauteren, I., Prinsen, E., Matosevich, R., Xu, J., Mironova, V., et al.** (2020). Rocks in the auxin stream: Wound-induced auxin accumulation and ERF115 expression synergistically drive stem cell regeneration. Proc Natl Acad Sci U S A **117**:16667-16677. 10.1073/pnas.2006620117.

**Casimiro, I., Marchant, A., Bhalerao, R.P., Beeckman, T., Dhooge, S., Swarup, R., Graham, N., Inze, D., Sandberg, G., Casero, P.J., et al.** (2001). Auxin transport promotes Arabidopsis lateral root initiation. Plant Cell **13**:843-852. 10.1105/tpc.13.4.843.

**Chaiwanon, J., and Wang, Z.Y.** (2015). Spatiotemporal brassinosteroid signaling and antagonism with auxin pattern stem cell dynamics in Arabidopsis roots. Curr Biol **25**:1031-1042. 10.1016/j.cub.2015.02.046.

**Ckurshumova, W., Smirnova, T., Marcos, D., Zayed, Y., and Berleth, T.** (2014). Irrepressible MONOPTEROS/ARF5 promotes de novo shoot formation. New Phytol **204**:556-566. 10.1111/nph.13014.

**Cole, M., Chandler, J., Weijers, D., Jacobs, B., Comelli, P., and Werr, W.** (2009). DORNROSCHEN is a direct target of the auxin response factor MONOPTEROS in the Arabidopsis embryo. Development **136**:1643-1651. 10.1242/dev.032177.

**Cornblatt, C.S., Shih, H.-W., and Monshausen, G.B.** (2021). Stimulus-specific processing of the plasma membrane receptor-like kinase FERONIA in <em>Arabidopsis thaliana</em&gt. bioRxiv:2021.2010.2008.463713. 10.1101/2021.10.08.463713.

**De Smet, I.** (2010). Multimodular auxin response controls lateral root development in Arabidopsis. Plant Signal Behav **5**:580-582. 10.4161/psb.11495.

**De Smet, I., Tetsumura, T., De Rybel, B., Frei dit Frey, N., Laplaze, L., Casimiro, I., Swarup, R., Naudts, M., Vanneste, S., Audenaert, D., et al.** (2007). Auxin-dependent regulation of lateral root positioning in the basal meristem of Arabidopsis. Development **134**:681-690. 10.1242/dev.02753.

**De Smet, I., Lau, S., Voss, U., Vanneste, S., Benjamins, R., Rademacher, E.H., Schlereth, A., De Rybel, B., Vassileva, V., Grunewald, W., et al.** (2010). Bimodular auxin response controls organogenesis in Arabidopsis. Proc Natl Acad Sci U S A **107**:2705-2710. 10.1073/pnas.0915001107.

**Ditengou, F.A., Teale, W.D., Kochersperger, P., Flittner, K.A., Kneuper, I., van der Graaff, E., Nziengui, H., Pinosa, F., Li, X., Nitschke, R., et al.** (2008). Mechanical induction of lateral root initiation in Arabidopsis thaliana. Proc Natl Acad Sci U S A **105**:18818-18823. 10.1073/pnas.0807814105.

**Dong, Q., Zhang, Z., Liu, Y., Tao, L.Z., and Liu, H.** (2019). FERONIA regulates auxin-mediated lateral root development and primary root gravitropism. FEBS Lett **593**:97-106. 10.1002/1873-3468.13292.

**Efroni, I., Mello, A., Nawy, T., Ip, P.L., Rahni, R., DelRose, N., Powers, A., Satija, R., and Birnbaum, K.D.** (2016). Root Regeneration Triggers an Embryo-like Sequence Guided by Hormonal Interactions. Cell **165**:1721-1733. 10.1016/j.cell.2016.04.046.

**Fendrych, M., Van Hautegem, T., Van Durme, M., Olvera-Carrillo, Y., Huysmans, M., Karimi, M., Lippens, S., Guerin, C.J., Krebs, M., Schumacher, K., et al.** (2014). Programmed cell death controlled by ANAC033/SOMBRERO determines root cap organ size in Arabidopsis. Curr Biol **24**:931-940. 10.1016/j.cub.2014.03.025.

**Feng, W., Kita, D., Peaucelle, A., Cartwright, H.N., Doan, V., Duan, Q., Liu, M.C., Maman, J., Steinhorst, L., Schmitz-Thom, I., et al.** (2018). The FERONIA Receptor Kinase Maintains Cell-Wall Integrity during Salt Stress through Ca(2+) Signaling. Curr Biol **28**:666-675 e665. 10.1016/j.cub.2018.01.023.

**Franck, C.M., Westermann, J., and Boisson-Dernier, A.** (2018). Plant Malectin-Like Receptor Kinases: From Cell Wall Integrity to Immunity and Beyond. Annu Rev Plant Biol **69**:301-328. 10.1146/annurev-arplant-042817-040557.

**Heyman, J., Canher, B., Bisht, A., Christiaens, F., and De Veylder, L.** (2018). Emerging role of the plant ERF transcription factors in coordinating wound defense responses and repair. J Cell Sci **131**10.1242/jcs.208215.

**Heyman, J., Cools, T., Vandenbussche, F., Heyndrickx, K.S., Van Leene, J., Vercauteren, I., Vanderauwera, S., Vandepoele, K., De Jaeger, G., Van Der Straeten, D., et al.** (2013). ERF115 controls root quiescent center cell division and stem cell replenishment. Science **342**:860-863. 10.1126/science.1240667.

**Heyman, J., Cools, T., Canher, B., Shavialenka, S., Traas, J., Vercauteren, I., Van den Daele, H., Persiau, G., De Jaeger, G., Sugimoto, K., et al.** (2016). The heterodimeric transcription factor complex ERF115-PAT1 grants regeneration competence. Nat Plants **2**:16165. 10.1038/nplants.2016.165.

**Hoermayer, L., Montesinos, J.C., Marhava, P., Benkova, E., Yoshida, S., and Friml, J.** (2020). Wounding-induced changes in cellular pressure and localized auxin signalling spatially coordinate restorative divisions in roots. Proc Natl Acad Sci U S A **117**:15322-15331. 10.1073/pnas.2003346117.

**Hofte, H.** (2015). The yin and yang of cell wall integrity control: brassinosteroid and FERONIA signaling. Plant Cell Physiol **56**:224-231. 10.1093/pcp/pcu182.

**Hofte, H., and Voxeur, A.** (2017). Plant cell walls. Curr Biol **27**:R865-R870. 10.1016/j.cub.2017.05.025.

**Holzwart, E., Huerta, A.I., Glockner, N., Garnelo Gomez, B., Wanke, F., Augustin, S., Askani, J.C., Schurholz, A.K., Harter, K., and Wolf, S.** (2018). BRI1 controls vascular cell fate in the Arabidopsis root through RLP44 and phytosulfokine signaling. Proc Natl Acad Sci U S A **115**:11838-11843. 10.1073/pnas.1814434115.

**Jürgens, T.B.a.G.** (1993). The role of the monopteros gene in organising the basal body region of

the Arabidopsis embryo. Development **118**:575-587.

**Karimi, M., Inze, D., and Depicker, A.** (2002). GATEWAY vectors for Agrobacterium-mediated plant transformation. Trends Plant Sci **7**:193-195. 10.1016/s1360-1385(02)02251-3.

**Kong, X., Tian, H., Yu, Q., Zhang, F., Wang, R., Gao, S., Xu, W., Liu, J., Shani, E., Fu, C., et al.** (2018). PHB3 Maintains Root Stem Cell Niche Identity through ROS-Responsive AP2/ERF Transcription Factors in Arabidopsis. Cell Rep **22**:1350-1363. 10.1016/j.celrep.2017.12.105.

**Koziol, A., Cybulska, J., Pieczywek, P.M., and Zdunek, A.** (2017). Changes of pectin nanostructure and cell wall stiffness induced in vitro by pectinase. Carbohydr Polym **161**:197-207. 10.1016/j.carbpol.2017.01.014.

**Krogan, N.T., Marcos, D., Weiner, A.I., and Berleth, T.** (2016). The auxin response factor MONOPTEROS controls meristem function and organogenesis in both the shoot and root through the direct regulation of PIN genes. New Phytol **212**:42-50. 10.1111/nph.14107.

**Kurihara, D., Mizuta, Y., Sato, Y., and Higashiyama, T.** (2015). ClearSee: a rapid optical clearing reagent for whole-plant fluorescence imaging. Development **142**:4168-4179. 10.1242/dev.127613.

**Lammens, T., Boudolf, V., Kheibarshekan, L., Zalmas, L.P., Gaamouche, T., Maes, S., Vanstraelen, M., Kondorosi, E., La Thangue, N.B., Govaerts, W., et al.** (2008). Atypical E2F activity restrains APC/CCCS52A2 function obligatory for endocycle onset. Proc Natl Acad Sci U S A **105**:14721-14726. 10.1073/pnas.0806510105.

**Lee, H.S., Kim, Y., Pham, G., Kim, J.W., Song, J.H., Lee, Y., Hwang, Y.S., Roux, S.J., and Kim, S.H.** (2015). Brassinazole resistant 1 (BZR1)-dependent brassinosteroid signalling pathway leads to ectopic activation of quiescent cell division and suppresses columella stem cell differentiation. J Exp Bot **66**:4835-4849. 10.1093/jxb/erv316.

**Lucas, M., Godin, C., Jay-Allemand, C., and Laplaze, L.** (2008). Auxin fluxes in the root apex co-regulate gravitropism and lateral root initiation. J Exp Bot **59**:55-66. 10.1093/jxb/erm171.

**Luo, L., Zeng, J., Wu, H., Tian, Z., and Zhao, Z.** (2018). A Molecular Framework for Auxin-Controlled Homeostasis of Shoot Stem Cells in Arabidopsis. Mol Plant **11**:899-913. 10.1016/j.molp.2018.04.006.

**Malamy, J.E., and Benfey, P. N.** (1997). Organization and cell differentiation in lateral roots of Arabidopsis thaliana. Development **124**:33-44.

**Marhava, P., Hoermayer, L., Yoshida, S., Marhavy, P., Benkova, E., and Friml, J.** (2019). Re-activation of Stem Cell Pathways for Pattern Restoration in Plant Wound Healing. Cell **177**:957-969 e913. 10.1016/j.cell.2019.04.015.

**Marhavy, P., Montesinos, J.C., Abuzeineh, A., Van Damme, D., Vermeer, J.E., Duclercq, J., Rakusova, H., Novakova, P., Friml, J., Geldner, N., et al.** (2016). Targeted cell elimination reveals an auxin-guided biphasic mode of lateral root initiation. Genes Dev **30**:471-483. 10.1101/gad.276964.115.

**Mehrnia, M., Balazadeh, S., Zanor, M.I., and Mueller-Roeber, B.** (2013). EBE, an AP2/ERF transcription factor highly expressed in proliferating cells, affects shoot architecture in Arabidopsis. Plant Physiol **162**:842-857. 10.1104/pp.113.214049.

**Melnyk, C.W.** (2017). Connecting the plant vasculature to friend or foe. New Phytol **213**:1611-1617. 10.1111/nph.14218.

**Melnyk, C.W., Schuster, C., Leyser, O., and Meyerowitz, E.M.** (2015). A Developmental Framework for Graft Formation and Vascular Reconnection in Arabidopsis thaliana. Curr Biol **25**:1306-1318. 10.1016/j.cub.2015.03.032.

**Melnyk, C.W., Gabel, A., Hardcastle, T.J., Robinson, S., Miyashima, S., Grosse, I., and Meyerowitz, E.M.** (2018). Transcriptome dynamics at Arabidopsis graft junctions reveal an intertissue recognition mechanism that activates vascular regeneration. Proc Natl Acad Sci U S A **115**:E2447-E2456. 10.1073/pnas.1718263115.

**Moller, B.K., Xuan, W., and Beeckman, T.** (2017). Dynamic control of lateral root positioning. Curr Opin Plant Biol **35**:1-7. 10.1016/j.pbi.2016.09.001.

**Moreno-Risueno, M.A., Van Norman, J.M., Moreno, A., Zhang, J., Ahnert, S.E., and Benfey, P.N.** (2010). Oscillating Gene Expression Determines Competence for Periodic Arabidopsis Root Branching. Science **329**:1306-1311. 10.1126/science.1191937.

**Parizot, B., Laplaze, L., Ricaud, L., Boucheron-Dubuisson, E., Bayle, V., Bonke, M., De Smet, I., Poethig, S.R., Helariutta, Y., Haseloff, J., et al.** (2008). Diarch symmetry of the vascular bundle in Arabidopsis root encompasses the pericycle and is reflected in distich lateral root initiation. Plant Physiol **146**:140-148. 10.1104/pp.107.107870.

**Pauwels, L., De Clercq, R., Goossens, J., Inigo, S., Williams, C., Ron, M., Britt, A., and Goossens, A.** (2018). A Dual sgRNA Approach for Functional Genomics in Arabidopsis thaliana. G3 (Bethesda) **8**:2603-2615. 10.1534/g3.118.200046.

**Perianez-Rodriguez, J., Manzano, C., and Moreno-Risueno, M.A.** (2014). Post-embryonic organogenesis and plant regeneration from tissues: two sides of the same coin? Front Plant Sci **5**:219. 10.3389/fpls.2014.00219.

**Pound, M.P., French, A.P., Atkinson, J.A., Wells, D.M., Bennett, M.J., and Pridmore, T.** (2013). RootNav: navigating images of complex root architectures. Plant Physiol **162**:1802-1814. 10.1104/pp.113.221531.

**Przemeck, G.K., Mattsson, J., Hardtke, C.S., Sung, Z.R., and Berleth, T.** (1996). Studies on the role of the Arabidopsis gene MONOPTEROS in vascular development and plant cell axialization. Planta **200**:229-237. 10.1007/bf00208313.

**Savatin, D.V., Gramegna, G., Modesti, V., and Cervone, F.** (2014). Wounding in the plant tissue: the defense of a dangerous passage. Front Plant Sci **5**:470. 10.3389/fpls.2014.00470.

**Schlereth, A., Moller, B., Liu, W., Kientz, M., Flipse, J., Rademacher, E.H., Schmid, M., Jurgens, G., and Weijers, D.** (2010). MONOPTEROS controls embryonic root initiation by regulating a mobile transcription factor. Nature **464**:913-916. 10.1038/nature08836.

**Schuetz, M., Berleth, T., and Mattsson, J.** (2008). Multiple MONOPTEROS-dependent pathways are involved in leaf initiation. Plant Physiol **148**:870-880. 10.1104/pp.108.119396.

**Sena, G., Wang, X., Liu, H.Y., Hofhuis, H., and Birnbaum, K.D.** (2009). Organ regeneration does not require a functional stem cell niche in plants. Nature **457**:1150-1153. 10.1038/nature07597.

**Shih, H.W., Miller, N.D., Dai, C., Spalding, E.P., and Monshausen, G.B.** (2014). The receptor-like kinase FERONIA is required for mechanical signal transduction in Arabidopsis seedlings. Curr Biol **24**:1887-1892. 10.1016/j.cub.2014.06.064.

**Smetana, O., Makila, R., Lyu, M., Amiryousefi, A., Sanchez Rodriguez, F., Wu, M.F., Sole-Gil, A., Leal Gavarron, M., Siligato, R., Miyashima, S., et al.** (2019). High levels of auxin signalling define the stem-cell organizer of the vascular cambium. Nature **565**:485-489. 10.1038/s41586-018-0837-0.

**Sun, S.B., Meng, L.S., Sun, X.D., and Feng, Z.H.** (2010). Using high competent shoot apical meristems of cockscomb as explants for studying function of ASYMMETRIC LEAVES2-LIKE11 (ASL11) gene of Arabidopsis. Mol Biol Rep **37**:3973-3982. 10.1007/s11033-010-0056-8.

**Ursache, R., Andersen, T.G., Marhavy, P., and Geldner, N.** (2018). A protocol for combining fluorescent proteins with histological stains for diverse cell wall components. Plant J **93**:399-412. 10.1111/tpj.13784.

**Vukasinovic, N., Wang, Y., Vanhoutte, I., Fendrych, M., Guo, B., Kvasnica, M., Jiroutova, P., Oklestkova, J., Strnad, M., and Russinova, E.** (2021). Local brassinosteroid biosynthesis enables optimal root growth. Nat Plants **7**:619-632. 10.1038/s41477-021-00917-x.

**Wang, Z.Y., Nakano, T., Gendron, J., He, J., Chen, M., Vafeados, D., Yang, Y., Fujioka, S., Yoshida, S., Asami, T., et al.** (2002). Nuclear-localized BZR1 mediates brassinosteroid-induced growth and feedback suppression of brassinosteroid biosynthesis. Dev Cell **2**:505-513. 10.1016/s1534-5807(02)00153-3.

**Wolf, S., Mravec, J., Greiner, S., Mouille, G., and Höfte, H.** (2012a). Plant cell wall homeostasis is mediated by brassinosteroid feedback signaling. Current Biology **22**:1732-1737. 10.1016/j.cub.2012.07.036.

**Wolf, S., Mravec, J., Greiner, S., Mouille, G., and Hofte, H.** (2012b). Plant cell wall homeostasis is mediated by brassinosteroid feedback signaling. Curr Biol **22**:1732-1737. 10.1016/j.cub.2012.07.036.

**Wolf, S., van der Does, D., Ladwig, F., Sticht, C., Kolbeck, A., Schurholz, A.K., Augustin, S., Keinath, N., Rausch, T., Greiner, S., et al.** (2014). A receptor-like protein mediates the response to pectin modification by activating brassinosteroid signaling. Proc Natl Acad Sci U S A **111**:15261-15266. 10.1073/pnas.1322979111.

**Xuan, W., Band, L.R., Kumpf, R.P., Van Damme, D., Parizot, B., De Rop, G., Opdenacker, D., Möller, B.K., Skorzinski, N., Njo, M.F., et al.** (2016). Cyclic programmed cell death stimulates hormone signaling and root development in Arabidopsis. Science **351**:384-387. 10.1126/science.aad2776.

**Yu, M., Li, R., Cui, Y., Chen, W., Li, B., Zhang, X., Bu, Y., Cao, Y., Xing, J., Jewaria, P.K., et al.** (2020). The RALF1-FERONIA interaction modulates endocytosis to mediate control of root growth in Arabidopsis. Development **147**10.1242/dev.189902.

**Zhang, A., Matsuoka, K., Kareem, A., Robert, M., Roszak, P., Blob, B., Bisht, A., De Veylder, L., Voiniciuc, C., Asahina, M., et al.** (2022). Cell-wall damage activates DOF transcription factors to promote wound healing and tissue regeneration in Arabidopsis thaliana. Curr Biol 10.1016/j.cub.2022.02.069.

**Zhou, W., Lozano-Torres, J.L., Blilou, I., Zhang, X., Zhai, Q., Smant, G., Li, C., and Scheres, B.** (2019). A Jasmonate Signaling Network Activates Root Stem Cells and Promotes Regeneration. Cell **177**:942-956 e914. 10.1016/j.cell.2019.03.006.

## Acknowledgements

The authors thank Annick Bleys for help in preparing the manuscript, Veronique De Storme and Marnik Vuylsteke for their contribution to statistical analyses, Frauke Augstein and Annelie Carlsbecker for scientific and intellectual contributions. This work was supported by grants (G007218N and G010820N) and a predoctoral fellowship (F.L.) from the Research Foundation-Flanders. AZ, SM and CWM were supported by a Wallenberg Academy Fellowship (2016-0274) and a Vetenskapsrådet grant (2017-05122).

**Author Contributions**

B.C. and L.D.V. wrote the manuscript. F.L and B.C performed LR phenotyping. BC performed luminescence imaging and phenotyping. A.Z and S.M performed the grafting assays. J.H and A.B performed CRISPR-Cas9 mutagenesis. S.W. and C.W.M. were involved in experimental design. All authors approved the manuscript.

**FIGURES**

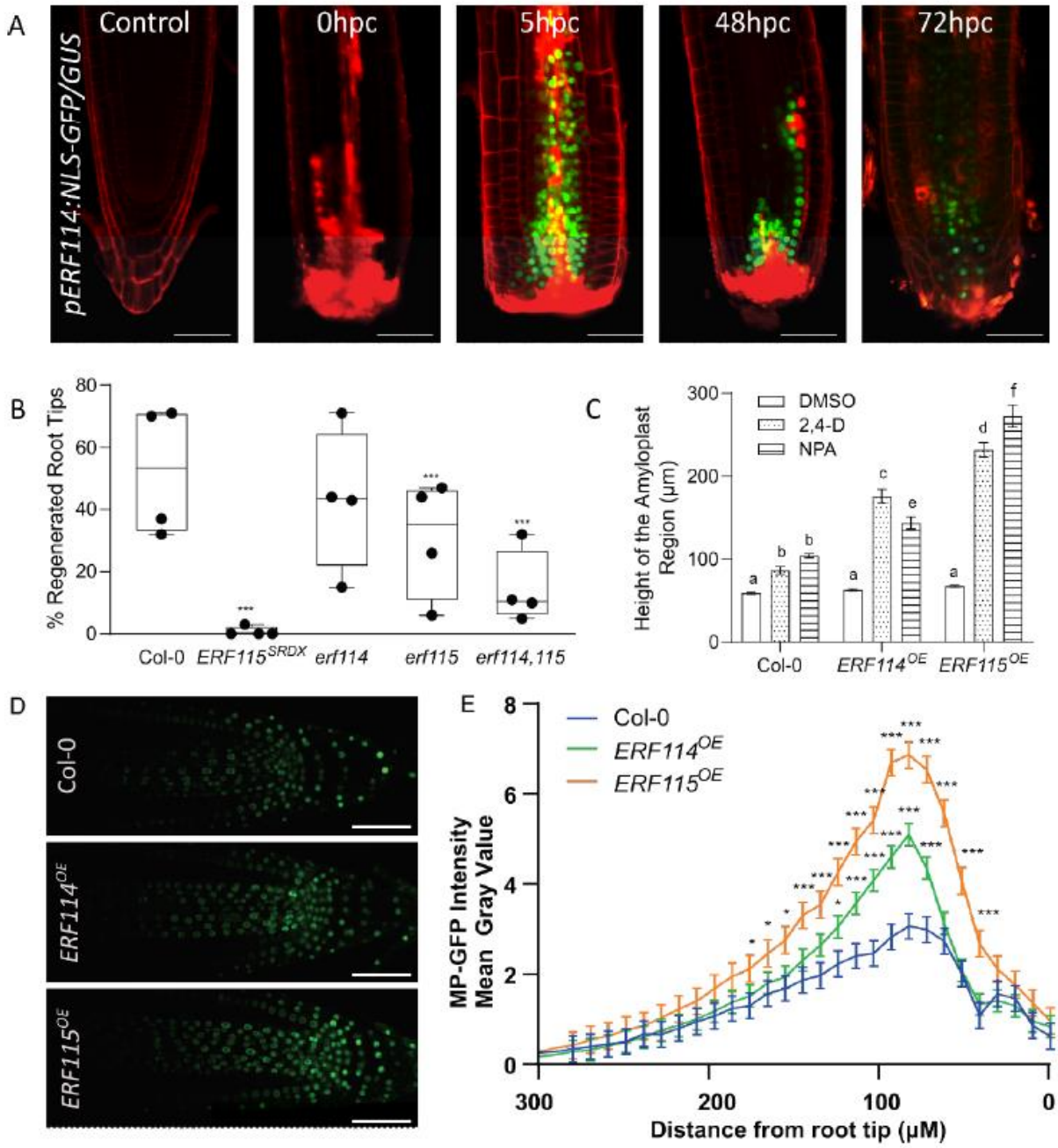


**Fig. 1 | ERF114 and ERF115 control root tip regeneration and confer auxin sensitivity A,** Confocal images of *pERF114:GFP-NLS/GUS* root tips (red) during regeneration from root tip excision (hpc = hours post cutting). Cell walls and dead cells are counterstained (red) with propidium Iodide (PI) Scalebars = 50 µm. **B,** Percentage of

regenerated root tips after stringent root tip excision. Error bars indicate standard error. Survival data was analyzed by a logistic regression. The significance of the difference with Col-0 for each genotype was calculated by a two-sided T-test followed by Bonferroni correction for multiple testing (***p < 0.001). **C,** Quantification of the amyloplast containing region size from seedlings grown 5 days on DMSO, NPA (10 µM) or 2,4-D (100 nM). **D,E,** Confocal images (D) of primary root tips holding *MP:MP-GFP* reporter in indicated backgrounds (F1 generation from crosses) and quantification of GFP intensity (E) per each 10 µm interval starting from the root tip. Scale bars = 50 µm. Wald tests were performed to determine genotype effects on signal intensity using a mixed model analysis with different regions were regarded as repeated measures (***p < 0.001). Means were compared using post-hoc testing followed by multiple testing adjustment using Bonferroni method.

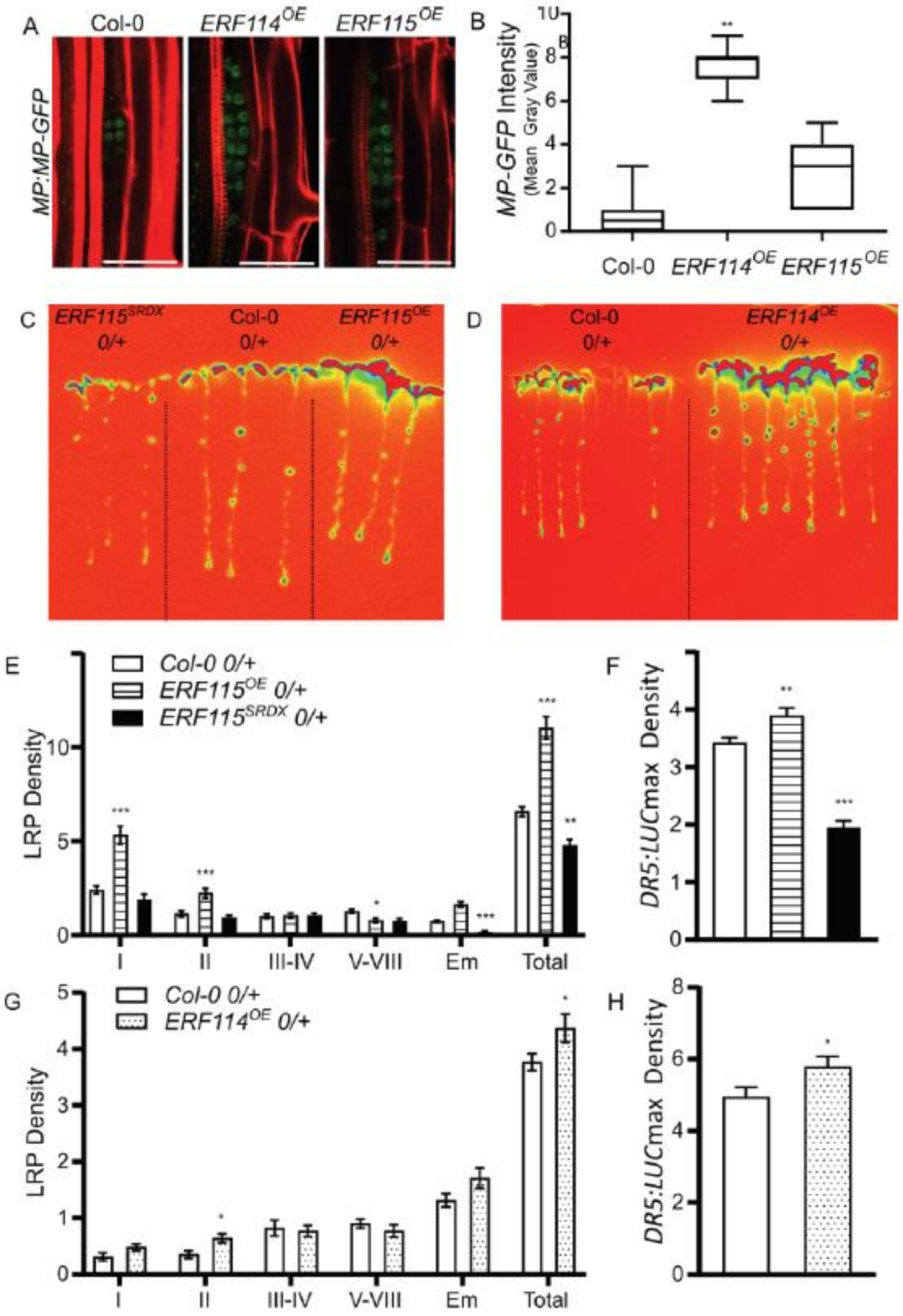
A
Col-0
ERF114OE
ERF115OE
MP:MP-GFP
B
MP-GFP Intensity
(Mean Gray Value)
Col-0
ERF114OE
ERF115OE
C
ERF115SRDX
0/+
Col-0
0/+
ERF115OE
0/+
D
Col-0
0/+
ERF114OE
0/+
E
Col-0 0/+
ERF115OE 0/+
ERF115SRDX 0/+
LRP Density
I
II
III-IV
V-VIII
Em
Total
F
DR5:LUCmax Density
G
Col-0 0/+
ERF114OE 0/+
LRP Density
I
II
III-IV
V-VIII
Em
Total
H
DR5:LUCmax Density

**Fig. 2 | ERF114 and ERF115 activate MP in correlation with increased lateral root formation A,** Confocal images of PI-stained stage II lateral root primordia (LRP) showing *MP:MP-GFP* in wild type (Col-0) and *ERF115*$^{OE}$ and *ERF114*$^{OE}$ backgrounds. Scale bars = 50 µm. **B,** Quantification of MP-GFP intensity as mean gray value from confocal images of stage II LRPs. **C**, Representative luminescence images of hemizygous F1 seedlings of *DR5:LUC* crossed with indicated genotypes. Brightness and contrast settings were adjusted for better visualization. **E-H,** LRP (E,G) and *DR5:LUC* maxima densities (no of DR5 maxima/cm) (F,H) of indicated genotypes crossed with *DR5:LUC* seedlings in the F1 generation (indicated as 0/+). Following luminescence imaging for DR5:LUC, LRP staging and quantification were performed from DIC images of the same seedlings after tissue clearing.

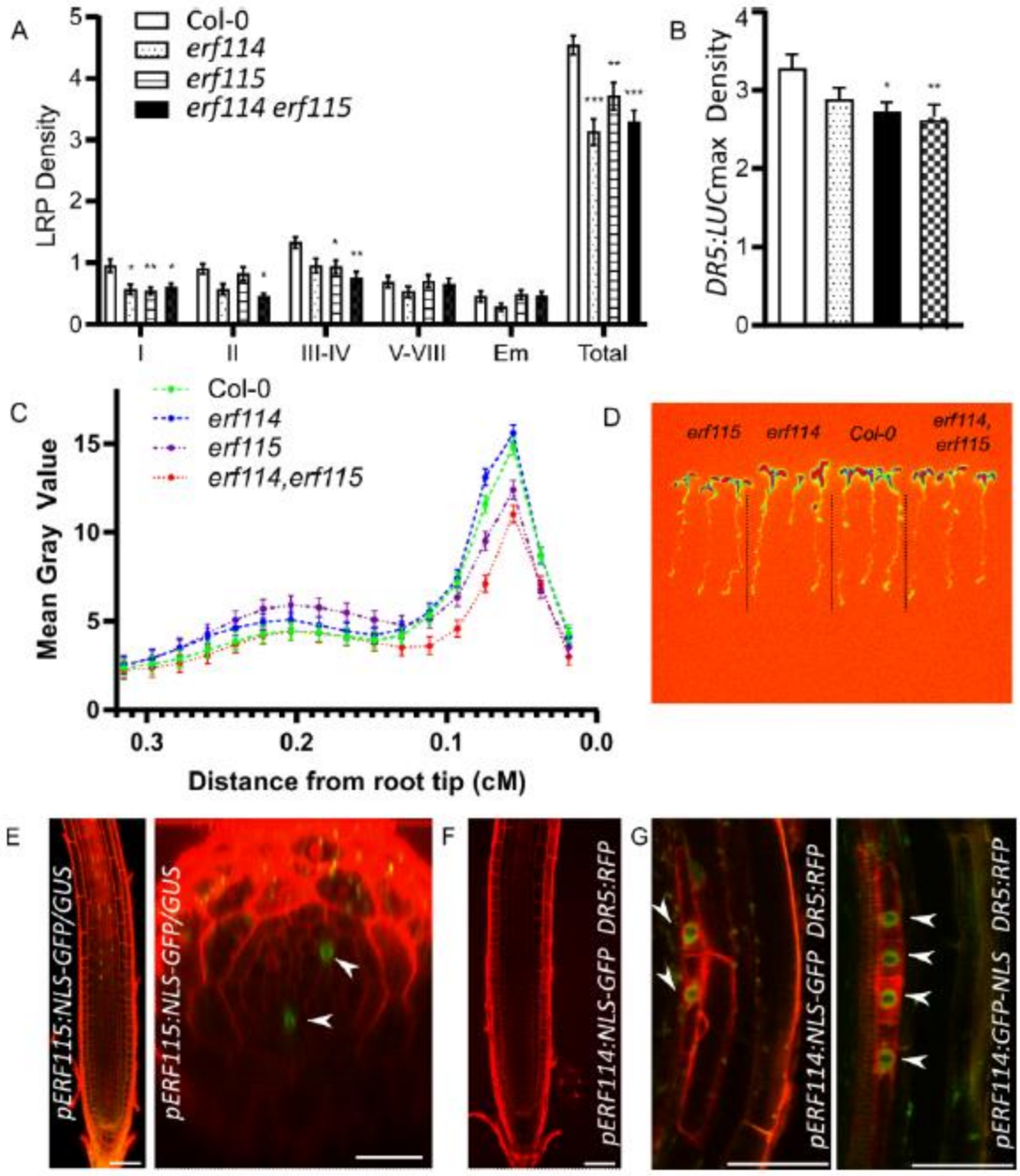


**Fig. 3 | ERF114 and ERF115 control lateral root primordia and contribute to auxin signaling intensity A-B** LRP (**A**) and DR5:LUC maxima densities (no of DR5 maxima/cm) (**B**) of homozygous *erf114*, *erf115* and *erf114 erf115* seedlings carrying *DR5:LUC* construct (*p < 0.05, **p < 0,01, ***p < 0.001 mixed model procedure was used to calculate significance values for pairwise comparisons with the wild type by least squares post-hoc tests and corrected for multiple testing using the Bonferroni Method).

**C**, Average *DR5:LUC* signal intensity plotted against distance from the root tip. The peak in the first 0.1 cm region corresponds to the meristematic auxin maxima. Wald tests were performed to determine genotype effects on signal intensity using a mixed model analysis with different regions were treated as repeated measures. **D**, Representative luminescence images of mutant lines holding *DR5:LUC* construct. **E**, Confocal image of *pERF115:GFP-NLS/GUS* root and cross section image showing protoxylem specific *ERF115* expression (indicated by arrowheads). **F,** Confocal image of *pERF114:GFP-NLS/GUS* primary meristem. **G**, Confocal images of *pERF114:GFP-NLS/GUS DR5:RFP* stained with PI showing *ERF114* expression in the LR founder cells (indicated by arrowheads).

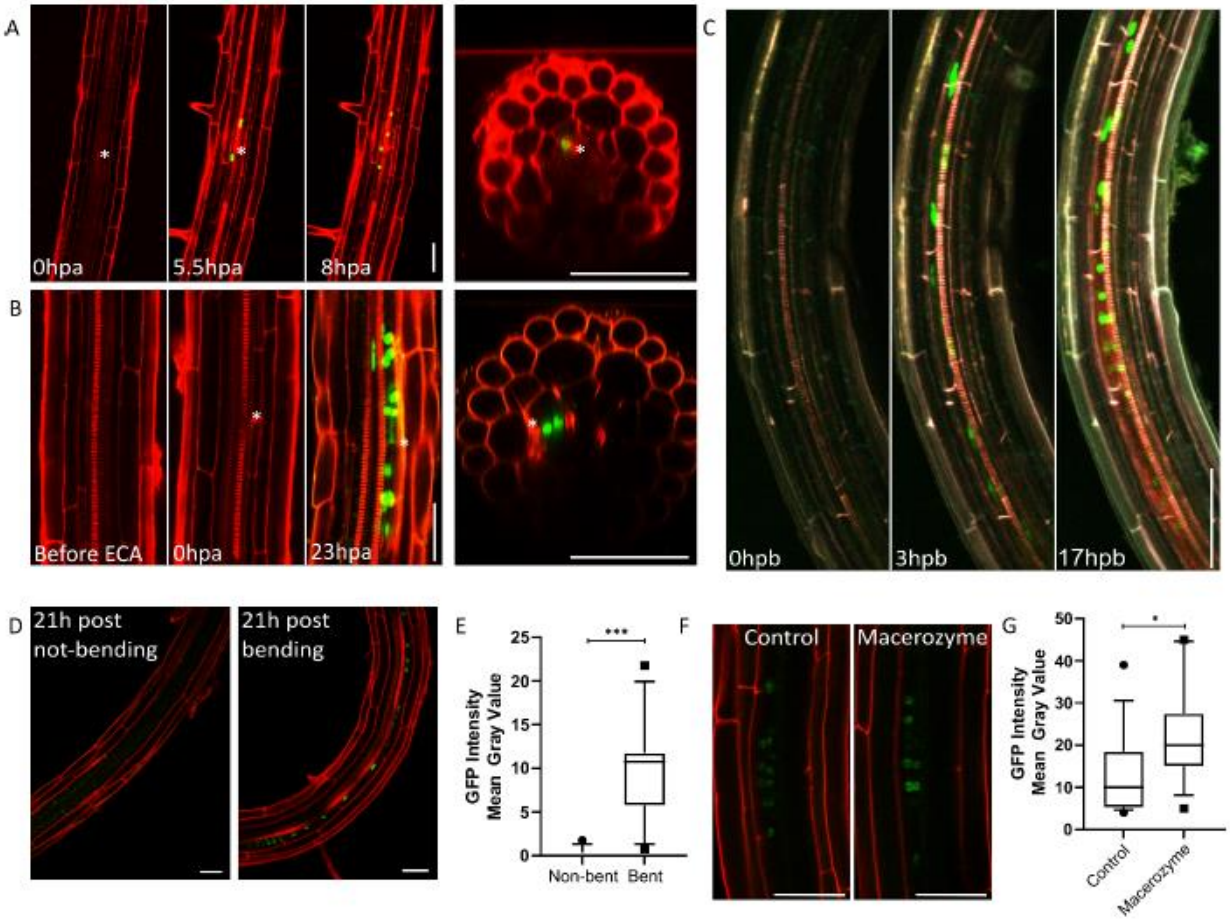


**Fig. 4**│ ***ERF114*** **responds to cell wall damage and mechanical stress. A-B,** Stills from time lapse imaging of PI stained (red) *pERF114:NLS-GFP/GUS* (green) seedlings after laser induced damaging of an immature protoxylem cell wall (Supplementary Movie 5) (A) or after endodermal cell ablation (B). Cross section images show *ERF114* expression in pericycle cells. Asterisks mark the point of laser exposure in the cell wall boundary between two protoxylem cells and ablated endodermal cell. **C,** Stills from time lapse imaging (Supplemental Movie 6) of PI-stained (cyan) *pERF114:NLS-GFP/GUS* (green) *DR5:RFP* (red) seedling after mechanical stress induced by root bending. hpa: hours post ablation hpb: hours post bending. **D**, Representative confocal images of PI stained (red) *pERF114:NLS-GFP/GUS* (green) seedlings 21h post bending or not bending. **E**, Quantification of GFP signal from bent region and the regions that were marked but not bent (Satterthwaite's T-test. ***$p < 0.01$). **F**, Representative confocal images of PI stained (red) *pERF114:NLS-GFP/GUS* (green) Stage II LRP after 24h of macerozyme (0.003%)

treatment vs control. **G**, Quantification of GFP intensity in control vs macerozyme treated Stage II LRPs (Satterthwaite's T-test *$p < 0.05$). All scale bars = 50 μm.

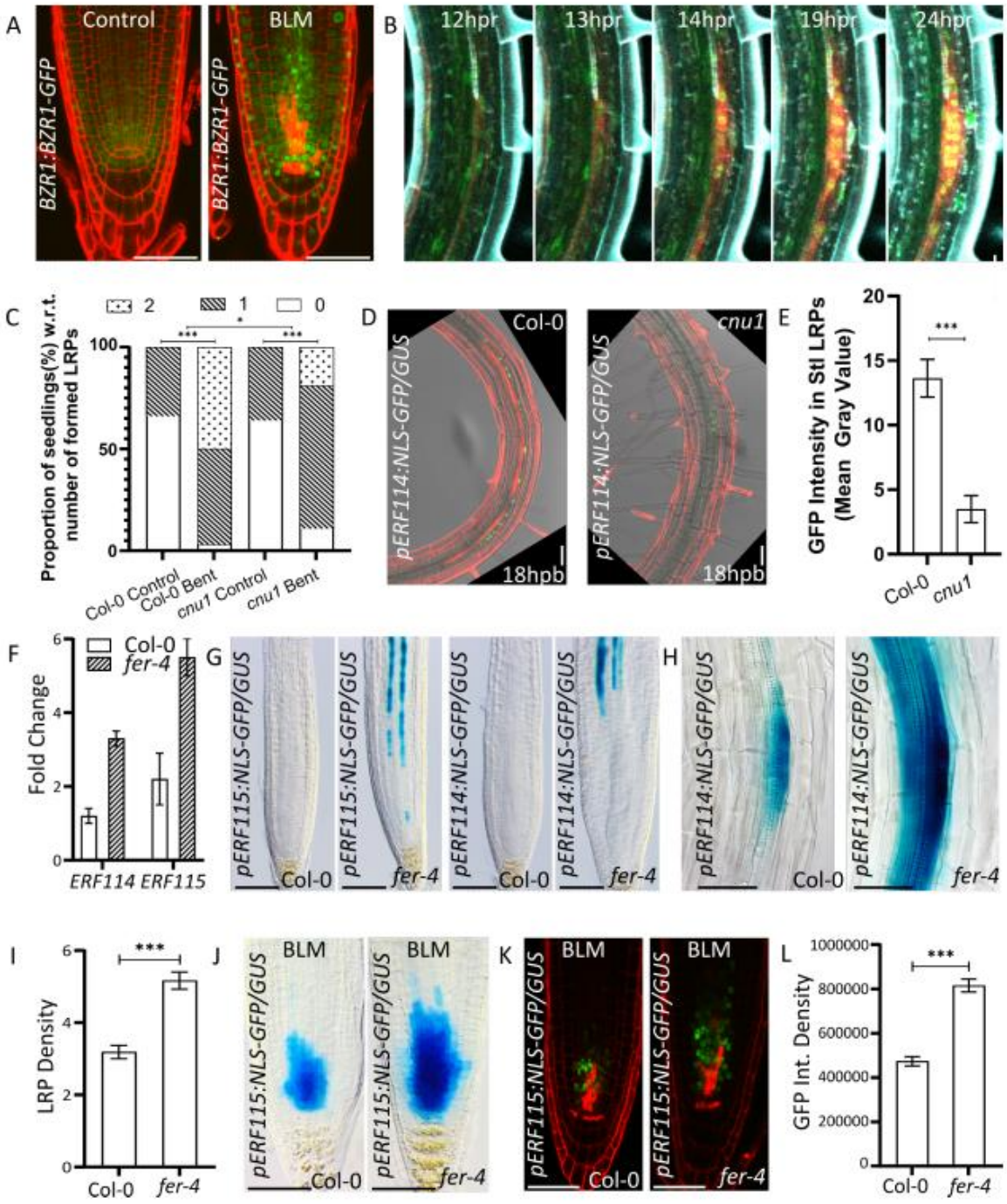


**Fig. 5 | *ERF114* and *ERF115* respond to cell wall mechanosensory signals. A,** *pBZR1:BZR1-GFP* expression under control conditions and after 24h BLM treatment (intense PI staining (red) indicates cell death). **B,** Time lapse imaging of PI stained (cyan) *BZR1:BZR1-GFP* (green) *DR5:RFP* (red) during LR formation. White arrowheads point

to LR founder cells and their daughters after anticlinal divisions **C**, Proportion of wild-type and *cnu1* seedlings with 0, 1 or 2 LRPs at the marked region 18 hours after no treatment (Control) or bending (Bent). **D,E**, Confocal images of *pERF114:NLS-GFP/GUS* reporter in wild-type or *cnu1* background 18 hours post bending (hpb) (D), and quantification of GFP signal indicating *ERF114* expression (E). **F,** Fold changes in *ERF114* and *ERF115* expression in wild type versus *fer-4* mutant roots as indicated by RT-qPCR. **G,H**, *ERF114* and *ERF115* expression in root tips (G) or early stage LRP (H) under control conditions in wild type versus *fer-4* mutant roots. **I,** LRP density of *fer-4* mutants (Satterthwaite's T-test. ***p < 0.01). **J,K**, GUS staining (J) and confocal imaging (K) of *pERF115:NLS-GFP/GUS* root tips after 24h of BLM treatment. Scale bars= 50 µm. **L,** Quantification of GFP integrated density of BLM treated *pERF115:NLS-GFP/GUS* root tips (Satterthwaite's T-test. ***p < 0.01).

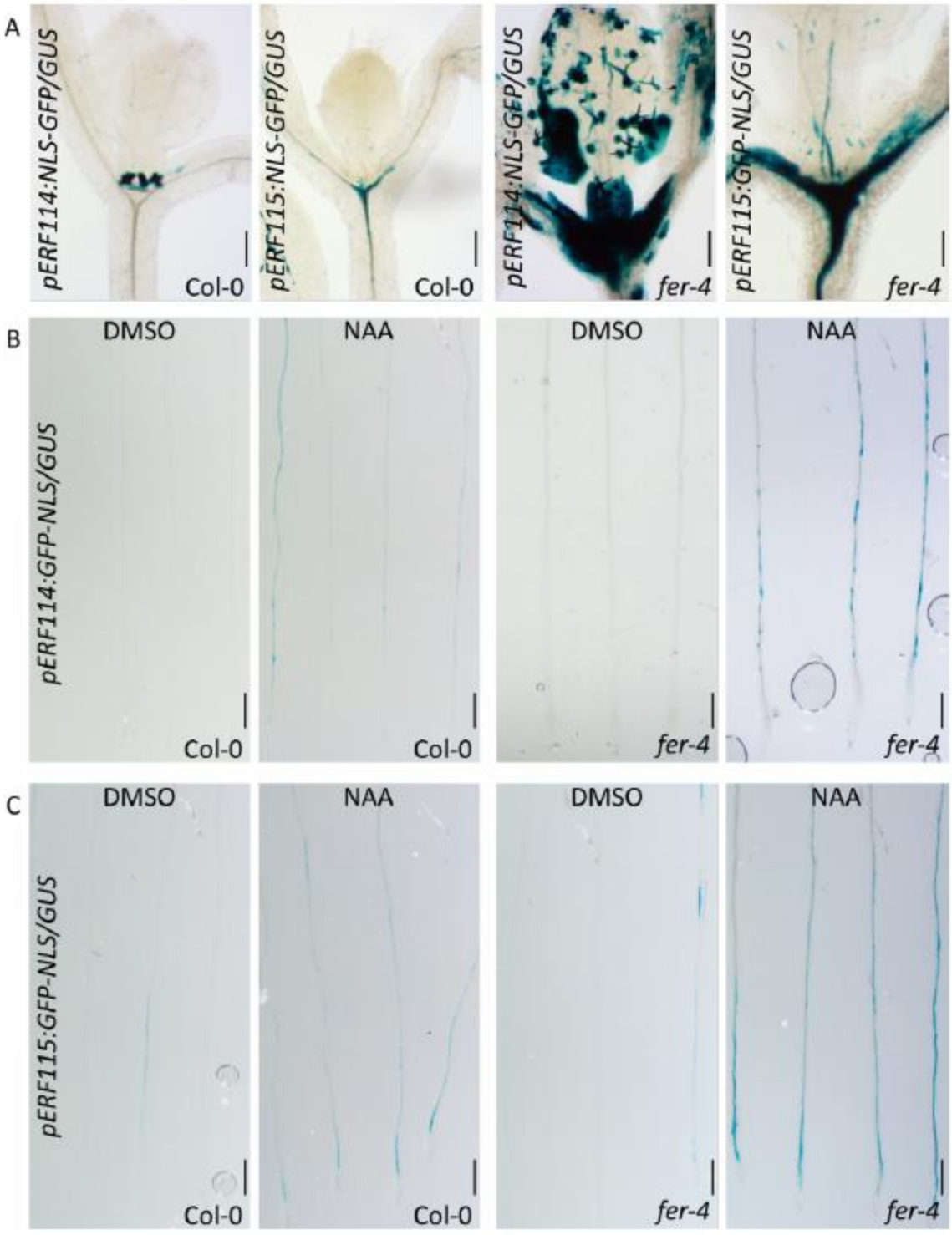


**Fig. 6. *fer*-4 mutants display increased *ERF114* and *ERF115* expression that can be enhanced by auxin treatment A**, Light microscopy images of GUS-stained *pERF114:GFP-NLS/GUS* and *pERF115:GFP-NLS/GUS* seedlings showing a stronger

expression in the *fer-4* background compared to Col-0. **B,C**, GUS staining of the roots of seedlings showing a stronger expression of *ERF114* (B) and *ERF115* (C) after treatment with NAA in the *fer-4* background compared to the wild type (Col-0). Scale bars = 100 µm.

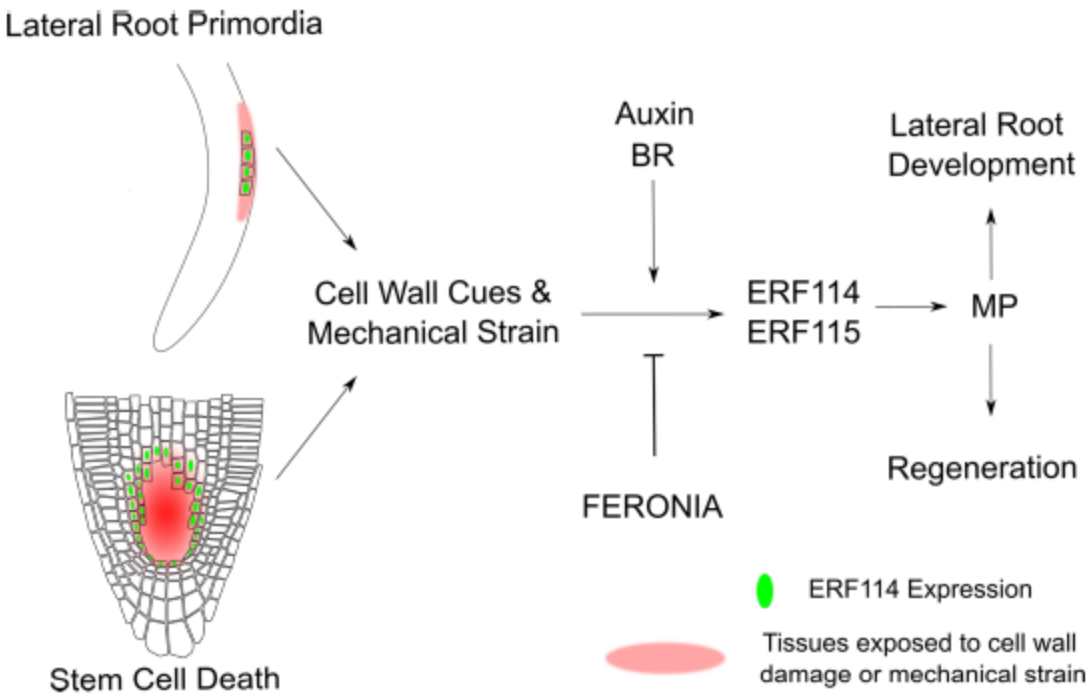


**Fig. 7. Model for cell wall cues and mechanical stress activating regeneration and lateral root development.** *ERF114* and *ERF115* are activated through cell wall cues and mechanical strains that is counteracted by FERONIA. Through subsequent activation of *MONOPTEROS* (*MP*), context dependent stem cell activation enables a regenerative or developmental response.